Title: CHIP disrupts monocyte-endothelial interactions across multiple tissues to promote vascular inflammation in humans

Authors: Alyssa C. Parker*[1], J. Brett Heimlich*[2], Ayesha Ahmad[3], Samuel S. Bailin[4], Joseph C. Van Amburg[1], Caitlyn Vlasschaert[5], John R. Koethe[4], Celestine N. Wanjalla MD PhD[+4], Alexander G. Bick MD PhD[+3]

*, [+] denotes equal contribution

Correspondence to Dr. Wanjalla (celestine.wanjalla@vumc.org) or Dr. Bick (alexander.bick@vumc.org)

Affiliations:

[1]Vanderbilt University School of Medicine, Nashville, TN 37232
[2]Division of Cardiovascular Medicine, Department of Medicine, Vanderbilt University Medical Center, Nashville, TN 37232
[3]Division of Genomic Medicine, Department of Medicine, Vanderbilt University Medical Center, Nashville, TN 37232
[4]Division of Infectious Diseases, Department of Medicine, Vanderbilt University Medical Center, Nashville, TN 37232
[5]Department of Medicine, Queen's University, Kingston Ontario, Canada

Abstract:

Background: Clonal hematopoiesis of indeterminate potential (CHIP) occurs when hematopoietic stem cells acquire mutations that confer a proliferative advantage. CHIP is associated with increased risk of multiple vascular diseases. Mouse models have identified CHIP monocytes as highly proinflammatory. Here we seek to build on these earlier studies by characterizing adipose tissue macrophages and vascular cells in patients with CHIP.

Methods: We performed single-cell RNA sequencing on paired peripheral blood mononuclear cells and subcutaneous adipose tissue from 6 CHIP patients and 6 matched controls. We analyzed cell type specific gene expression profiles and intercellular interactions.

Results: We found that macrophages had an exaggerated proinflammatory profile compared to circulating monocytes. We also found increased interaction between circulating CD14+ monocytes and endothelial cells. Specifically, cells from patients with CHIP showed enhanced signaling related to leukocyte transendothelial migration. These differences were tissue specific. We recapitulated monocyte-endothelial cell interactions in single cell RNA sequencing data from a mouse model of CHIP.

Conclusions: Monocytes from patients with CHIP have increased endothelial interaction compared to controls and macrophages from patients with CHIP are highly proinflammatory. Alterations in the monocyte-endothelial interaction in CHIP likely contribute to cardiovascular disease risk.

Introduction:

Clonal hematopoiesis of indeterminate potential (CHIP) occurs when hematopoietic stems cells acquire mutations in leukemia-associated genes conferring a proliferative advantage to those stem cells. Mutant hematopoietic stem cells give rise to mutated blood cell populations. CHIP can be initiated by mutations in more than 50 genes, but approximately two-thirds of all CHIP cases are driven by mutations in just two genes: DNA Methyltransferase 3A (*DNMT3A*) and Tet Methylcytosine Dioxygenase 2 (*TET2*).

CHIP has been associated with a diverse set of cardiac and vascular diseases, including coronary artery disease, peripheral vascular disease, vascular dementia, and heart failure[1–5]. Hypercholesterolemic mouse models of *TET2* and *DNMT3A* have highlighted the critical role of inflammatory pathways in disease pathogenesis[4,6,7]. Mice that receive bone marrow transplants containing *Tet2* knockout cells develop significantly larger atherosclerotic lesions than control mice[4]. Additionally, bone marrow-derived macrophages from *Tet2* knockout mice have significant upregulation of inflammatory cytokines and chemokines, including *Cxcl1, Cxcl2, Cxcl3, Pf4, Il1b,* and *Il6*[4,7]*.* Evidence of increased inflammation in these mice is also present in spleen, kidney, liver, and lung in the form of xanthomas, foam cell accumulation, and inflammatory infiltrates[4].

CHIP studies involving multiomic characterization of human subjects to date have principally focused on the peripheral blood[8–13]. Recent single-cell RNA sequencing (scRNAseq) studies of human CHIP samples have established that CHIP affects the inflammatory state of blood cells, most significantly CD14+ monocytes[8,9,11,12]. Lineage tracing has allowed comparison of mutant and wildtype cells, demonstrating both cell-intrinsic and cell-extrinsic effects of CHIP mutations in monocytes and T cells. These studies have highlighted significant upregulation of key cytokines and inflammasome components in monocytes from patients with CHIP and more specifically in monocytes that carry CHIP mutations.

Although blood is a highly convenient tissue, it does not capture critical aspects of CHIP vascular pathology, such as macrophages or the vasculature itself. Peripheral adipose tissue, a highly vascularized tissue, offers a unique window into the vasculature. Recent work on the effect of infectious diseases on metabolism has made use of peripheral adipose tissue to evaluate gene expression and cell type proportions[14]. We hypothesized that adipose tissue samples may similarly provide insight into the effects of CHIP on the vasculature. CHIP has been associated with adipose-related phenotypes including insulin resistance and increased BMI[1,15,16], suggesting that vascular related consequences of CHIP may be observable in adipose tissue.

In this study, we report for the first time that CHIP alters the interaction of blood immune cells with vascular endothelial cells in human patients. We used scRNAseq to characterize the molecular landscapes of blood and adipose tissue biopsies taken from CHIP patients at the same clinic visit. We found that CHIP is associated with upregulation of key molecules related to leukocyte capture in endothelial cells. We replicated these observations in a mouse model. Additionally, within the myeloid lineage, we identified more differentially expressed genes in macrophages from adipose tissue than in monocytes from blood. Lastly, our evaluation of interactions between endothelial cells from various vascular beds and macrophages from patients with CHIP identified significant heterogeneity between vascular beds. Together these observations provide a more complete understanding of how CHIP contributes to vascular pathology in human patients and highlights potential therapeutic strategies for these patients.

Methods:

Samples for this study came from 12 participants from the HIV, Adipose Tissue Immunology, and Metabolism study (NCT04451980) [14], including 6 patients with CHIP and 6 controls. All individuals provided informed consent and the study was approved by the Vanderbilt University Medical Center Institutional Review Board. CHIP status was identified using a previously described targeted sequencing assay[17]. Controls were matched based on age, sex, and HIV/diabetic status. 10 of the samples were from HIV-negative participants with diabetes. The remaining two samples came from HIV-positive, prediabetic participants. Adipose tissue biopsies and blood samples were taken at the same clinic visit. scRNAseq yielded data for 73,790 cells, averaging 6,149 cells per person. See Supplemental Methods for further details.

Data for the mouse monocyte-endothelial cell signaling prediction experiment was extracted from publicly available datasets. Monocyte data was obtained from a published CHIP mouse model[18]. Endothelial cell data was obtained from The Tabula Muris Consortium[19] through the CZI CELLxGENE database. Data for the human monocyte-endothelial cell signaling prediction experiment was extracted from a prior CHIP scRNAseq study[8]. Endothelial cells were obtained from the CZI CELLxGENE database using the census.

Differential expression and pathway analysis was performed using a metacells approach in which reads from cells in similar transcriptional states were collapsed into single measurements to overcome issues with sparsity and prevent false discovery. Intercellular signaling was predicted based on ligand-receptor gene expression levels using CellChat[20]. Transcription factor activity was evaluated using decoupleR, based on the CollecTRI network[21]. Interactor scoring for individual cells was determined based on expression of marker genes. We used the top 10 markers that defined high and low interacting endothelial tissues and then calculated an interaction likelihood score for each cell.

Results:

To understand the interactions between peripheral blood containing cells with CHIP mutations and vascular tissue, we collected both peripheral blood mononuclear cells (PBMCs) and adipose tissue biopsies from 6 patients with CHIP and 6 controls (**Fig. 1A**, **Table 1**). scRNAseq yielded data for a total of 73,790 cells. We identified distinct populations of immune cells in both PBMCs and in adipose tissue (**Fig. 1B, Supplemental Fig. 1**). To understand how signaling between blood cells and vascular tissue changes with CHIP, we predicted intercellular signaling using CellChat. Across all cell types, we found that intercellular signaling was most enhanced for interactions with endothelial cells, specifically for interactions with adipose tissue CD8+ T cells and circulating CD14+ monocytes (**Fig. 1C**). We also observed that intercellular signaling in CHIP was most diminished for interactions with macrophages.

CHIP macrophage gene expression reflects transcription factor activity in mutant CD14+ monocytes

The two CHIP driver genes considered in this analysis, *TET2* and *DNMT3A*, are both involved in DNA methylation and have been found to play a cooperative role in regulating expression of transcription factors[22]. For this reason, we were interested in evaluating transcription factor activity amongst CHIP and control cells. We performed transcription factor enrichment analysis on CHIP patient CD14+ monocytes that have been labeled with mutation status in a study by

Heimlich et al[8]. We identified a set of transcription factors that were more active in mutant cells, including myelocytomatosis oncogene (MYC) and signal transducer and activator of transcription 6 (STAT6) (**Fig. 2A**). MYC plays an important role in hematopoiesis and is often activated in acute myeloid leukemia[23,24]. STAT6 is the major transcription factor responsible for inducing macrophage M2 polarization[25]. Downstream differential expression of target genes for these transcription factors followed expectations. For example, *HLA*-A, *HLA-C*, *HLA-E*, *VAMP2*, *ICAM1*, *CXCL2*, *CXCL8*, and *FOS* are targets of MYC and were significantly upregulated in macrophages from patients with CHIP compared to controls (adj p-value < 0.05, **Supplementary Table 1**). Similarly, *CXCL8*, *JAK1*, *DUSP1*, *FOS*, *MRC1*, *CD4*, and *CD86* are targets of STAT6 and were all significantly upregulated in macrophages from patients with CHIP compared to controls (adj p-value < 0.05, **Supplementary Table 1**). We also identified a set of transcription factors that were less active in mutant cells, including *NR1H3* and *NR1H4*. In macrophages from patients with CHIP, targets of NR1H3, *APOE* and *CD36*, were significantly downregulated (adj p-value < 0.05, **Supplementary Table 1**). Targets of NR1H4, *MMP9*, *APOE*, *CD36*, and *SUMO1*, were also significantly downregulated in macrophages from patients with CHIP (adj p-value < 0.05, **Supplementary Table 1**).

Macrophages from patients with CHIP have more differentially expressed genes compared to controls than circulating CD14+ monocytes

Previous analyses of CHIP have mainly focused on effects of CHIP on peripheral blood[8,9,11,12]. Here, we took advantage of having access to both peripheral blood and adipose tissue to compare the effects of CHIP in both compartments. We observed very few differentially expressed genes in circulating CD14+ monocytes, compared to what we observed in adipose tissue macrophages from matched sample pairs (**Fig. 2B, Supplementary Table 1-2**). In the macrophage analyses, we observed several differentially expressed genes involved in transendothelial migration, including vesicle associated membrane protein 2 (*VAMP2)* and intercellular adhesion molecule 1 (*ICAM1)* (log2(fold change) = 0.49, adj p-value = 2.02×10^{-5}; log2(fold change) = 0.53, adj p-value = 4.83×10^{-4}). We also observed significant upregulation of human leukocyte antigen (HLA) types, *HLA-A*, *HLA-C*, and *HLA-E,* in macrophages from patients with CHIP compared to controls (log2(fold change) = 0.74, adj p-value = $2.7.80 \times 10^{-13}$; log2(fold change) = 0.61, adj p-value = 7.19×10^{-11}; log2(fold change) = 0.54, adj p-value = 3.04×10^{-9}). Gene set enrichment analysis explained that while cellular energy production was largely unaffected by CHIP in circulating CD14+ monocytes, oxidative phosphorylation and mitochondrial function were significantly suppressed in macrophages (**Fig. 2C, Supplementary Fig. 2)**.

Transendothelial migration signaling enhanced in endothelial cells from CHIP patients compared to controls

Differential expression analysis of endothelial cells from CHIP patients and controls identified that, as seen in macrophages, several HLA types were significantly upregulated with CHIP, namely *HLA-A*, *HLA-C*, *HLA-B* (log2(fold change) = 0.448, adj p-value = 5.92×10^{-49}; log2(fold change) = 0.802, adj p-value = 1.10×10^{-47}; log2(fold change) = 0.619, adj p-value = 1.88×10^{-39}, **Supplementary Table 3**). Additionally, important regulators of transendothelial migration were upregulated in endothelial cells from patients with CHIP, specifically vesicle associated membrane protein 3 (*VAMP3*), platelet and endothelial cell adhesion molecule 1 (*PECAM1*), and plasmalemma vesicle associated protein (*PLVAP*) (log2(fold change) = 0.285, adj p-value = 2.44×10^{-5}; log2(fold change) = 0.410, adj p-value = 2.16×10^{-5}; log2(fold change) = 0.458, adj p-

value = 0.01, **Supplementary Table 3**) (**Fig. 3A**). The process of monocyte transendothelial migration includes chemokine/cytokine-directed attraction, selectin-dependent tethering/rolling, integrin-dependent adhesion, and adhesion molecule-dependent migration across the endothelial cell barrier (**Fig 3B**). Dysregulation of transendothelial migration is implicated in inflammatory disease processes, including vascular diseases[26]. CellChat predictions of circulating CD14+ monocyte and endothelial cell interactions highlighted multiple transendothelial migration signaling pathways that differ in signaling strength between CHIP and control. A dominant signal from circulating CD14+ monocytes to endothelial cells was present in CHIP for each step of transendothelial migration: chemokine (C-X-C motif) ligand (CXCL) for cytokine-directed attraction, L-selectin (SELL) for selectin-dependent tethering, integrin subunit beta 2 (ITGB2) for integrin-dependent adhesion, and platelet and endothelial cell adhesion molecule 1 (PECAM1) for adhesion molecule-dependent migration across the endothelial barrier (**Fig. 3C-F**). In comparing signaling strength between CHIP and control samples, there was a statistically significantly higher signal for each of these pathways in CHIP (p-value < 0.0125) (**Fig. 3G**).

We replicated this signal in the CHIP mouse model by analyzing mouse monocytes from *Tet2* KO and control mice in conjunction with mouse endothelial cells. Signaling molecules involved in transendothelial migration do not perfectly correlate between humans and mice, so we could not directly compare pathways. For example, IL8 is one of the central components of CXCL signaling in humans but the mouse homologs KC, MIP-1, and LIX do not function in the same way and therefore cannot be compared[27]. However, the general process of leukocyte transendothelial migration involves similar steps that can be compared. As in humans, cytokine and selectin signaling, denoted here by tumor necrosis factor (TNF) and selectin P ligand gene (SELPLG), were increased with CHIP in mice (**Fig. 3H**). Integrin signaling, denoted here by integrin alpha L-integrin subunit beta 2 (ITGAL-ITGB2), was increased in mice with CHIP but did not reach statistical significance. Transforming growth factor-β (TGFβ) signaling, which plays a role in mice similar to PECAM1's role in humans by regulating the cadherin-dependent endothelial barrier permeability, was significantly higher in mice with CHIP than in wildtype mice. Overall, these simulations suggested that CHIP in mice and humans is characterized by increases in transendothelial migration signaling.

Macrophages from patients with CHIP have enhanced signaling to endothelial cells

We used CellChat to predict how macrophages from patients with CHIP and from controls interact with endothelial cells (**Fig. 4A**). We evaluated differential signaling strength between macrophages and endothelial cells for three transendothelial migration pathways (CXCL, ITGB2, and PECAM1) that align with three of the four steps of transendothelial migration: chemokine/cytokine signaling, integrin binding, and adhesion molecule migration (**Fig. 4B**). We did not observe any selectin signaling in these cells so could not perform that comparison. Each of the three pathways we evaluated had statistically significantly higher signaling in CHIP compared to controls.

High heterogeneity in interactions between macrophages and endothelial cells across tissues

Although there are vascular beds in nearly every tissue in the body, CHIP causes disease in specific vascular beds[2,28]. To investigate the origin of differential interactions between CHIP blood and endothelial cells throughout the body, we extracted endothelial cell gene expression data from 15 unique tissues from the Chan Zuckerberg Initiative (CZI) CELLxGENE database[29].

Endothelial cell identity was verified using expression of known endothelial marker genes (**Supplementary Fig. 3**). We predicted signaling strength between macrophages from patients with CHIP and endothelial cell populations using CellChat (**Fig. 4C**). There was high heterogeneity in the interaction of endothelial cells with macrophages, depending on the tissue of origin. We ranked tissues based on the strength of their interactions with CHIP macrophages (**Fig. 4D**). The top interacting tissues included spleen, liver, and endometrium. Low interacting tissues included lung, heart right ventricle, and heart left ventricle.

To determine factors contributing to interaction strength, we calculated cluster defining markers for endothelial cells from high interactor and low interactor tissues. Top markers of high interactors included albumin (*ALB*), serpin family E member 1 (*SERPINE1*), and NF-kappa-B inhibitor alpha (*NFKBIA*) (adj p-value < $0.05x10^{-10}$, **Supplementary Table 4**). Top markers of low interactors included protein tyrosine phosphatase receptor type M (*PTPRM*), endomucin (*EMCN*), and MDS and EVI1 complex locus (*MECOM*) (adj p-value < $0.05x10^{-10}$, **Supplementary Table 4**). To compare high and low interacting endothelial cells within CHIP patients, we used the cluster defining markers to classify individual endothelial cells from the CHIP adipose tissue data. An interaction score was calculated for each cell using gene expression multiplied by the rank order of top marker genes. The top 500 cells were classified as high interactors, and the bottom 500 cells were classified as low interactors. We then characterized differences in transcription factor activity between high and low interactors. We identified many transcription factors that were more active amongst the high interactors including Jun proto-oncogene (*JUN*), JunD proto-oncogene (*JUND*), and regulatory factor X associated protein (*RFXAP*), important regulators of cytokine release and MHC class II presentation[30,31](**Fig. 4E**). As we might expect based on activity of these transcription factors, CXCL signaling between macrophages and high interactor endothelial cells was enhanced compared to signaling between macrophages and low interactor endothelial cells (**Fig. 4F**). Upon further review of high and low interactor endothelial cells, we found that observed counts of endothelial cell subtypes within high interactor and low interactor groups varied. A generalized linear model of the effect of endothelial cell subtype and sample of origin on high interactor proportion suggested that venous endothelial cell status is a positive predictor of high interactor proportion with a coefficient of 0.461, standard error of 0.138, and p-value of 0.004. No other endothelial cell subtype or sample of origin was a statistically significant predictor of high interactor proportion (**Fig. 4G**).

Discussion:

Here we conduct the first multi-tissue scRNAseq analysis of CHIP in humans, using samples from peripheral blood and adipose tissue. By simultaneously sampling peripheral blood and adipose tissue from CHIP cases and controls, we demonstrate that endothelial cells from patients with CHIP have significant upregulation of key molecules related to leukocyte transendothelial migration. We characterize effects of CHIP on myeloid cells, which vary greatly depending on the location in the body. We also demonstrate that vascular disease-relevant effects may be limited to tissues with endothelial cells that have high likelihood of interacting with macrophages. These findings permit several conclusions.

First, CHIP affects gene expression of key molecules related to leukocyte capture in endothelial cells. CHIP is known to affect the vasculature, as it has been associated with higher risk of coronary artery disease, peripheral artery disease, and atherosclerosis[1,3,28]. Additionally, studies in mice have shown that CHIP endothelial cells overexpress P-selectin and recruit monocytes more readily[4]. However, this is the first study to evaluate changes to gene expression and

signaling patterns in human endothelial cells from patients with CHIP. We identified upregulation of *VAMP3*, *PECAM1*, and *PLVAP*, all key molecules involved in transendothelial migration, in endothelial cells from patients with CHIP.

Second, within the myeloid lineage, we identified more differentially expressed genes in macrophages from adipose tissue than in monocytes from blood. Most CHIP studies to date have focused on peripheral blood and have found differences related to inflammatory signaling. While these findings are supported by our data, we demonstrate that more significant and disease-relevant differences are found in peripheral tissues, emphasizing the importance of evaluating CHIP in tissues beyond blood. We found that adipose tissue macrophages from patients with CHIP had upregulation of genes favoring transendothelial migration, including *VAMP2* and *ICAM1*, as well as several *HLA* types. Murine models of *TET2* CHIP have similarly demonstrated a differentiation bias towards proinflammatory MHCII^{+} macrophages[32,33]. Because this study did not evaluate mutation status of macrophages, future work will be needed to clarify the extent to which macrophages in human adipose tissue carry CHIP mutations.

Third, our evaluation of the interaction between macrophages and endothelial cells in CHIP demonstrated that there is a heterogenous response across tissues. We observed that macrophage interactions with endothelial cells differ in strength according to the endothelial tissue of origin. Highest signaling strength was observed in the spleen and liver, tissues that have high levels of sinusoidal endothelial cells which express MHC receptors and have high leukocyte permeability[34,35]. High interactor endothelial cells from the CHIP adipose dataset demonstrated high activity of transcription factors related to MHC class II presentation. It is possible that the differential response of endothelial cells across tissues contributes to the variability of disease risk across tissues. Notably, prior work has demonstrated effects of CHIP on these highly interacting tissues. Specifically, mouse models of CHIP develop splenomegaly as excess immune cells accumulate in the spleen[16,33]. Future work investigating drug targets for CHIP may benefit from tissue-specific evaluation.

Our study has several limitations that we have attempted to address. Our cohort consists mainly of patients with obesity. For this reason, some inflammatory markers may already be upregulated, even in the absence of CHIP. We addressed this by matching cases and controls by diabetic status, as described in the methods. Obesity could also mask some of the inflammatory response triggered by CHIP, as obesity contributes to inflammation. Therefore, observations related to inflammation are likely to be conservative and repeating this study in non-obese individuals is likely to identify greater differences.

In conclusion, our study suggests that in addition to initiating an inflammatory response in the blood, CHIP affects the function of endothelial cells and disrupts regulation of monocyte transendothelial migration. This deeper understanding of signaling patterns suggests a specific biological pathway that may be targeted in therapies to address vascular disease risks associated with CHIP.

Supplemental methods:

Patient attainment and inclusion criteria

Samples were taken from participants in the HIV, Adipose Tissue Immunology, and Metabolism (HATIM) study, designed to characterize adipose tissue in the context of HIV infection and metabolic disease (ClinicalTrials.gov registration NCT04451980). Patients with HIV (PWH) were

recruited from the Vanderbilt University Medical Center Comprehensive Care Clinic between August 2017 and June 2018. All were on antiretroviral therapy (ART) for ≥ 18 months, had virologic suppression (serum HIV-1 RNA quantification < 50 copies/mL) for ≥ 12 months, had a $CD4^+$ T cell count ≥ 350 cells/mm at enrollment and had no known inflammatory or rheumatologic conditions. Patients were further classified as non-diabetic (HbA1c < 5.7% and/or fasting blood glucose [FBG] < 100 mg/dL), pre-diabetic (HbA1c 5.7-6.5% and/or FBG 100-125 mg/dL), or diabetic (HbA1c > 6.4% and/or FBG ≥ 126 mg/dL and/or on anti-diabetic medication) in accordance with the American Diabetes Association criteria. HIV-negative patients with diabetes were recruited from the Vanderbilt *ResearchMatch* cohort. These patients were matched by age and BMI with diabetic PWH. Before sample collection, all patients underwent a minimum 8-hour fast. PBMCs and subcutaneous adipose tissue were then collected. The project was approved by the Vanderbilt Institutional Review Board (IRB # 161254), and all patients provided written consent. From this cohort, patients were evaluated for CHIP status. Six patients with CHIP and six controls matched for age, sex, HIV status, and diabetic status were selected for this study. Adipose tissue and PBMCs were collected from all patients.

CHIP variant calling

Samples from all patients underwent targeted sequencing to identify the presence of CHIP driver mutations. DNA extraction from whole blood was performed using Qiagen Mini kits Cat #27104, following standard procedures. Samples were then sequenced on an Illumina Novaseq 6000 using a custom gene panel designed to target CHIP driver genes with 600x read depth as previously described[10,17]. Putative somatic mutations were identified using the Mutect2-GATK package, and filtering was applied to identify variants that met previously defined criteria for CHIP[36]. Variants with total low read depth (<100), low variant allele read depth (<3) and/or variant allele fraction below the threshold for CHIP (<2%) were removed from the dataset.

Subcutaneous adipose tissue biopsies

Biopsies from subcutaneous adipose tissue (SAT) were collected approximately 3 cm to the right of the umbilicus after anesthetizing the skin with lidocaine/epinephrine and infiltrating 40 mL of sterile saline and lidocaine into the SAT. Approximately 5 grams of adipose tissue were collected using a 2.1 mm blunt, side-ported liposuction catheter (Tulip CellFriendly™GEMS system Miller Harvester, Tulip Medical Products). This method results in droplets of adipose tissue, typically < 3 mm in diameter. The samples were then placed in 40-50 mm of cold saline and mixed. Visible blood clots were removed. Samples were then transferred to a 70 µm filter for repeat saline washes with constant stirring. The adipose tissue was then placed in a gentleMACS™ Dissociator (Miltenyi Biotec) followed by incubation with 100 µL of collagenase D (20mg/mL). The SVF was separated using a Ficoll-Paque Plus density gradient. Samples were cryopreserved in fetal bovine serum with 10% DMSO in liquid nitrogen.

Single-cell RNA sequencing (PBMCs)

Cryopreserved PBMCs were thawed at 37°C then washed with complete RPMI (RPMI + 10% FBS + 1% PS, cRPMI) to remove the freezing media. An aliquot of 500,000 cells from each sample was plated with phosphate-buffered saline and incubated for 4.5 hours at 37°C and 5% CO_2. Cells were then pooled with unique hashtag antibody oligonucleotide-conjugates (HTOs) for 30 minutes (Biolegend, TotalSeq-B). Samples were then prepared with a 10X Chromium 3' library preparation kit (10X Genomics) and immediately run on a 10X Chromium Controller to create scRNAseq libraries.

Single-cell RNA sequencing (adipose tissue)

An antibody Total Seq C master mix was prepared using 0.5 µL each of 45 markers for lineage, memory and activation. Samples for this study were prepared in a larger group of samples in which 12 samples were processed at a time. Samples were thawed and transferred to 15 mL tubes then diluted to 10 mL with phosphate-buffered saline. They were then spun down at 300 G for 10 minutes. The supernatant was aspirated, and the pellet was resuspended in cell staining buffer. Samples were transferred to flow tubes and spun at 300 G for 10 minutes. The supernatant was aspirated, and cells were resuspended in 100 µL of staining buffer. The tubes each received 5 µL of Human TruStain FcX Receptor Blocking Solution and were incubated at 4°C for 10 minutes. The antibody master mix was spun at 15,000 rpm for 5 minutes to remove aggregates and then 22.5 µL of master mic was added to each tube of cells, followed by mixing with flicking. Each tube received 1 µL of Total Seq C hashtag antibody and was then incubated at 4°C for 30 minutes. The cells were then washed with Cell Staining Buffer 3 times and spun at 300 G for 10 minutes. Cells were resuspended in 100 µL of PBS with 0.04% bovine serum albumin. Cells were counted using the Countess II Automated Cell Counter (Thermo Fisher) to calculate the suspension volume to transfer to obtain 5,000 cells. Samples were then pooled after being labeled with unique hashtag antibodies. Pooling was done by metabolic status in groups of four. Non-diabetic and prediabetic samples from PWH were pooled together. Multiplexed cells were then loaded onto a Chromium Single Cell 5' v.2 assay (10X Genomics).

scRNAseq data processing and cell type annotation

Next-generation 150-nt paired-end sequenced was performed on an Illumina Novaseq6000. Resulting bcl files were demultiplexed using bcl2fastq. Reads were aligned to the human genome (hg38) using STAR version 2.7.2a and cells were called using CellRanger from 10X Genomics with default parameters. Downstream analysis was performed in R (v4.3.2) on Terra.bio. To improve assignment of cells to donors, we used Souporcell (v2.0), which genetically demultiplexes samples using single nucleotide variants[37]. Ambient RNA was removed using the R package SoupX (v1.6.2)[38] and Seurat (v5.0.1)[39] objects were created. Cells with greater than 25% mitochondrial reads, <800 total transcripts, or <200 genes were filtered out. Doublets were identified using the R package DoubletFinder (v2.0.3)[40]. Cells lacking HTOs were removed. HTOs were used as ground truth for doublet identification. The doublet formation rate was set to (dim(seurat_object)[2]/0.57) * 4.6e-6, based on doublet formation rates predicted by the Satija lab (satijalab.org/costpercell).

Processed lanes were merged. HTO and DoubletFinder-predicted doublets were removed. Remaining hemoglobin, X chromosome, mitochondrial, and ribosomal genes were removed. Gene counts were normalized using the NormalizeData() function, followed by FindVariableFeatures() with nFeatures = 3000. Counts were scaled with the ScaleData() function, and dimensionality reduction was performed with the functions RunPCA() and RunUMAP() with dims = 1:15. We corrected batch effects with the R package Harmony (0.1.1)[41] and calculated clusters with the Seurat functions FindNeighbors() and FindClusters(). Annotation of cell types was performed with scType[42] for PBMCs and with manual annotation for adipose tissue cells. One cluster of PBMCs had high levels of mitochondrial DNA and low transcript and gene counts, suggesting that it captured a population of dead or dying cells. This cluster was removed from the analysis.

Differential expression and pathway analysis

scRNAseq analysis is complicated by frequent dropout from high levels of sparsity. We used a metacells approach in which reads from cells in similar transcriptional states were collapsed into single measurements. Metacell assignments were determined using the Python (v3.10.11) package Metacell-2 (v0.8.0)[43]. Metacells were classified within disease-state and cell type groups. Gene counts for each metacell were summed into a single value using the function aggregateAcrossCells(). Genes that had at least 10 transcripts in 85% of metacells were considered for downstream analysis. Differential expression was calculated with a negative binomial Wald test and Benjamini Hochberg p-value adjustment from the R package DESeq2 (1.40.2)[44].

Pathway analysis was performed based on differential expression results using the function gseGO() from the R package clusterProfiler (4.8.1)[45]. The dataset of pathways used was the "ALL" set from the GO database. Minimum gene set size was set to 2 and maximum gene set size was set to 800. The number of permutations calculated was 10,000.

Intercellular signaling prediction

Cell signaling was predicted using the R package CellChat (v1.6.1)[20]. CellChat uses a reference database of ligand-receptor interactions from peer-reviewed literature and other public signaling databases to estimate the likelihood of cell-cell interactions. The standard protocol was followed to create CellChat objects. The value for min.cells in filterCommunication was set to 25. For comparisons between groups, statistical significance was evaluated using the rankNet() function with do.stat = TRUE. This function performs a paired Wilcoxon test to evaluate whether there is a significant difference between the groups. The p-value threshold for significance was set using the Bonferroni method in which 0.05 was divided by the number of signaling pathways being evaluated.

Mouse validation of monocyte-endothelial cell signaling patterns

Data for the mouse monocyte-endothelial cell signaling prediction experiment was extracted from publicly available datasets. Monocyte data was obtained from a CHIP model mouse study[18]. Endothelial cell data was obtained through the CZI CELLxGENE database from The Tabula Muris Consortium[19]. Cell type annotations were assigned for the monocyte data using to original authors' publicly available code. Only cells labeled as "Monocytes" were included in this analysis. Endothelial cell data was subset to cells that had been annotated by original authors with the labels "endothelial cell," "vein endothelial cell," "endothelial cell of lymphatic vessel," "endothelial cell of coronary artery," "kidney capillary endothelial cell," and "endothelial cell of hepatic sinusoid." The data was merged, normalized and scaled with the function SCTransform(), and then passed to CellChat for signaling prediction. The standard process was followed for generating CellChat objects. Signaling was predicted from monocytes to endothelial cells using CellChat.

Signaling predictions for interactions between macrophages and endothelial cells

We predicted signaling from macrophages to endothelial cells from 15 unique tissues using publicly available data from the CZI CELLxGENE database. Data was obtained using the R package cellxgene.census (v1.8.0)[29]. The census database version used was "2023-07-25." Cells were requested that fit the following filters: organism = "Homo sapiens," cell type = "endothelial cell," assay = "10x 3' v3," and disease = "normal." Cells were verified to be endothelial cells using known endothelial cell marker genes, including *ICAM1*, *PECAM1*, *CD34*, and *VWF*. Only cell types that had at least 645 cells and appreciable expression of endothelial

cell markers were included. The endothelial dataset was downsampled to 645 cells per tissue and merged with macrophages from this study (downsampled to 2700 cells from patients with CHIP and from controls). The data was then normalized and scaled using the function SCTransform(). The standard process was followed for generating CellChat objects and performing predictions.

Transcription factor enrichment

Two evaluations of transcription factor activity were performed: one between mutant and wildtype CD14+ monocytes and one between high and low interactor endothelial cells. For the mutant and wildtype monocyte comparison, we isolated CD14+ monocytes from a single-cell analysis of CHIP that separated based on mutation status[8]. For the endothelial cell comparison, we used the top 500 high interactor and the top 500 low interactor endothelial cells from the adipose tissue samples from CHIP patients in this study. Transcription factor activity was evaluated using the R package decoupleR (v2.6.0)[21]. Data being evaluated was normalized and scaled using the function SCTransform() then analyzed using the function run_wmean() with the parameters times = 100 and minsize = 5. The network of transcription factors evaluated was pulled from the CollecTRI network, using the function get_collectri().

CHIP adipose tissue endothelial cell interactor scoring and comparison

High and low interacting tissues were defined from a ranked list of overall interaction strength outgoing from macrophages from patients with CHIP, incoming to endothelial cells from adipose tissue, accessible through cellchat_obj@net$weight. The highest five tissues were classified as high interacting tissues, and the lowest five tissues were classified as low interacting tissues. To understand gene expression patterns that defined high and low interactions, we subset endothelial cells to those from high and low interacting tissues then calculated cluster-defining markers using a Wilcoxon rank sum test as performed by the function FindAllMarkers() with parameters of logfc.threshold = 0.5, min.pct = 0.25, and assay = “SCT.” The set of markers was filtered to exclude mitochondrial and ribosomal genes.

We were interested in comparing high and low interacting cells from our CHIP adipose tissue endothelial cell data. To do so, we used the top 10 markers that defined high and low interacting tissues and calculated an interaction likelihood score. For each cell, gene expression of the marker was multiplied by the marker’s rank + 1. Markers for high interaction were added and markers for low interaction were subtracted to calculate a final score. The 500 cells with the highest score were classified as high interactors and the 500 cells with the lowest score were classified as low interactors. A CellChat object was created with the standard process and comparisons were made between high and low interactors.

Visualization

Visualization of data was primarily completed with the R package ggplot2 (v3.4.4)[46]. All schematics were prepared using BioRender.com. Colors were drawn from the R package RColorBrewer (v1.1-3)[47], Paired palette.

Sources of funding:

This study was funded by the following: K23DK135414 (SSB, JRK), Doris Duke CSDA 2021193 (CNW), K23 HL156759 (CNW), Burroughs Wellcome Fund 1021480 (CNW), R01 DK112262

(JRK), the Tennessee Center for AIDS Research grant P30 AI110527 (Supplement CNW, JK), the Vanderbilt Flow Cytometry Shared Resource is supported by the Vanderbilt Ingram Cancer Center (P30 CA068485). This work was also supported by NIH Early Independence Award grant DP5 OD029586, a Burroughs Wellcome Fund Career Award for Medical Scientists, a Pew-Stewart Scholar for Cancer Research award, supported by the Pew Charitable Trusts and the Alexander and Margaret Stewart Trust (AGB).

Disclosures:

AGB is a scientific co-founder of TenSixteen Bio.

References:

1. Jaiswal, S. *et al.* Age-related clonal hematopoiesis associated with adverse outcomes. *N. Engl. J. Med.* **371**, 2488–2498 (2014).
2. Yu, Z. *et al.* Genetic modification of inflammation- and clonal hematopoiesis–associated cardiovascular risk. *J. Clin. Invest.* **133**, (2023).
3. Bonnefond, A. *et al.* Association between large detectable clonal mosaicism and type 2 diabetes with vascular complications. *Nat. Genet.* **45**, 1040–1043 (2013).
4. Jaiswal, S. *et al.* Clonal Hematopoiesis and Risk of Atherosclerotic Cardiovascular Disease. *N. Engl. J. Med.* **377**, 111–121 (2017).
5. Bouzid, H. *et al.* Clonal hematopoiesis is associated with protection from Alzheimer's disease. *Nat. Med.* **29**, 1662–1670 (2023).
6. Fuster, J. J. *et al.* Clonal hematopoiesis associated with TET2 deficiency accelerates atherosclerosis development in mice. *Science* **355**, 842–847 (2017).
7. Fuster, J. J. *et al.* TET2-Loss-of-Function-Driven Clonal Hematopoiesis Exacerbates Experimental Insulin Resistance in Aging and Obesity. *Cell Rep.* **33**, 108326 (2020).
8. Heimlich, J. B. *et al.* Multiomic Profiling of Human Clonal Hematopoiesis Reveals Genotype and Cell-Specific Inflammatory Pathway Activation. 2022.12.01.518580 Preprint at https://doi.org/10.1101/2022.12.01.518580 (2023).

9. Nam, A. S. *et al.* Single-cell multi-omics of human clonal hematopoiesis reveals that DNMT3A R882 mutations perturb early progenitor states through selective hypomethylation. *Nat. Genet.* **54**, 1514–1526 (2022).
10. Miller, T. E. *et al.* Mitochondrial variant enrichment from high-throughput single-cell RNA sequencing resolves clonal populations. *Nat. Biotechnol.* 1–5 (2022) doi:10.1038/s41587-022-01210-8.
11. Abplanalp, W. T. *et al.* Association of Clonal Hematopoiesis of Indeterminate Potential With Inflammatory Gene Expression in Patients With Severe Degenerative Aortic Valve Stenosis or Chronic Postischemic Heart Failure. *JAMA Cardiol.* **5**, 1170–1175 (2020).
12. Abplanalp, W. T. *et al.* Cell-intrinsic effects of clonal hematopoiesis in heart failure. *Nat. Cardiovasc. Res.* **2**, 819–834 (2023).
13. Choi, B. *et al.* Single-cell transcriptome analyses reveal distinct gene expression signatures of severe COVID-19 in the presence of clonal hematopoiesis. *Exp. Mol. Med.* **54**, 1756–1765 (2022).
14. Bailin, S. S. *et al.* Changes in subcutaneous white adipose tissue cellular composition and molecular programs underlie glucose intolerance in persons with HIV. *Front. Immunol.* **14**, (2023).
15. Haring, B. *et al.* Healthy Lifestyle and Clonal Hematopoiesis of Indeterminate Potential: Results From the Women's Health Initiative. *J. Am. Heart Assoc.* **10**, e018789 (2021).
16. Pasupuleti, S. K. *et al.* Obesity-induced inflammation exacerbates clonal hematopoiesis. *J. Clin. Invest.* **133**, e163968 (2023).
17. Mack, T. *et al.* Cost-effective and scalable clonal hematopoiesis assay provides insight into clonal dynamics. *MedRxiv Prepr. Serv. Health Sci.* 2023.11.08.23298270 (2023) doi:10.1101/2023.11.08.23298270.

18. Rauch, P. J. *et al.* Loss-of-function mutations in Dnmt3a and Tet2 lead to accelerated atherosclerosis and concordant macrophage phenotypes. *Nat. Cardiovasc. Res.* **2**, 805–818 (2023).
19. Almanzar, N. *et al.* A single-cell transcriptomic atlas characterizes ageing tissues in the mouse. *Nature* **583**, 590–595 (2020).
20. Jin, S. *et al.* Inference and analysis of cell-cell communication using CellChat. *Nat. Commun.* **12**, 1088 (2021).
21. Badia-i-Mompel, P. *et al.* decoupleR: ensemble of computational methods to infer biological activities from omics data. *Bioinforma. Adv.* **2**, vbac016 (2022).
22. Zhang, X. *et al.* DNMT3A and TET2 compete and cooperate to repress lineage-specific transcription factors in hematopoietic stem cells. *Nat. Genet.* **48**, 1014–1023 (2016).
23. Hoffman, B., Amanullah, A., Shafarenko, M. & Liebermann, D. A. The proto-oncogene c-myc in hematopoietic development and leukemogenesis. *Oncogene* **21**, 3414–3421 (2002).
24. Salvatori, B. *et al.* Critical Role of c-Myc in Acute Myeloid Leukemia Involving Direct Regulation of miR-26a and Histone Methyltransferase EZH2. *Genes Cancer* **2**, 585–592 (2011).
25. Yu, T. *et al.* Modulation of M2 macrophage polarization by the crosstalk between Stat6 and Trim24. *Nat. Commun.* **10**, 4353 (2019).
26. Ridker, P. M. *et al.* Antiinflammatory Therapy with Canakinumab for Atherosclerotic Disease. *N. Engl. J. Med.* **377**, 1119–1131 (2017).
27. Hol, J., Wilhelmsen, L. & Haraldsen, G. The murine IL-8 homologues KC, MIP-2, and LIX are found in endothelial cytoplasmic granules but not in Weibel-Palade bodies. *J. Leukoc. Biol.* **87**, 501–508 (2010).
28. Zekavat, S. M. *et al.* TP53-mediated clonal hematopoiesis confers increased risk for incident atherosclerotic disease. *Nat. Cardiovasc. Res.* 1–15 (2023) doi:10.1038/s44161-022-00206-6.

29. Cellxgene Data Portal. *Cellxgene Data Portal* https://cellxgene.cziscience.com/.

30. Durand, B. *et al.* RFXAP, a novel subunit of the RFX DNA binding complex is mutated in MHC class II deficiency. *EMBO J.* **16**, 1045–1055 (1997).

31. Combined ChIP-Seq and transcriptome analysis identifies AP-1/JunD as a primary regulator of oxidative stress and IL-1β synthesis in macrophages | BMC Genomics | Full Text. https://bmcgenomics.biomedcentral.com/articles/10.1186/1471-2164-14-92.

32. Yeaton, A. *et al.* The Impact of Inflammation-Induced Tumor Plasticity during Myeloid Transformation. *Cancer Discov.* **12**, 2392–2413 (2022).

33. McClatchy, J. *et al.* Clonal hematopoiesis related TET2 loss-of-function impedes IL1β-mediated epigenetic reprogramming in hematopoietic stem and progenitor cells. *Nat. Commun.* **14**, 8102 (2023).

34. Shetty, S., Lalor, P. F. & Adams, D. H. Liver sinusoidal endothelial cells — gatekeepers of hepatic immunity. *Nat. Rev. Gastroenterol. Hepatol.* **15**, 555–567 (2018).

35. Steiniger, B. S. Human spleen microanatomy: why mice do not suffice. *Immunology* **145**, 334–346 (2015).

36. Vlasschaert, C. *et al.* A practical approach to curate clonal hematopoiesis of indeterminate potential in human genetic data sets. *Blood* **141**, 2214–2223 (2023).

37. Heaton, H. *et al.* Souporcell: robust clustering of single-cell RNA-seq data by genotype without reference genotypes. *Nat. Methods* **17**, 615–620 (2020).

38. Young, M. D. & Behjati, S. SoupX removes ambient RNA contamination from droplet-based single-cell RNA sequencing data. *GigaScience* **9**, giaa151 (2020).

39. Hao, Y. *et al.* Dictionary learning for integrative, multimodal and scalable single-cell analysis. *Nat. Biotechnol.* 1–12 (2023) doi:10.1038/s41587-023-01767-y.

40. *DoubletFinder: DoubletFinder Is a Suite of Tools for Identifying Doublets in Single-Cell RNA Sequencing Data.* (2022).

41. Korsunsky, I. *et al.* Fast, sensitive and accurate integration of single-cell data with Harmony. *Nat. Methods* **16**, 1289–1296 (2019).

42. Ianevski, A., Giri, A. K. & Aittokallio, T. Fully-automated and ultra-fast cell-type identification using specific marker combinations from single-cell transcriptomic data. *Nat. Commun.* **13**, 1246 (2022).

43. Ben-Kiki, O., Bercovich, A., Lifshitz, A. & Tanay, A. Metacell-2: a divide-and-conquer metacell algorithm for scalable scRNA-seq analysis. *Genome Biol.* **23**, 100 (2022).

44. Love, M. I., Huber, W. & Anders, S. Moderated estimation of fold change and dispersion for RNA-seq data with DESeq2. *Genome Biol.* **15**, 550 (2014).

45. Wu, T. *et al.* clusterProfiler 4.0: A universal enrichment tool for interpreting omics data. *Innov. Camb. Mass* **2**, 100141 (2021).

46. Wickham, H. *Ggplot2: Elegant Graphics for Data Analysis*. (Springer-Verlag New York, 2016).

47. Neuwirth, E. RColorBrewer: ColorBrewer Palettes. (2022).

Figure legends:

Figure 1: Single-cell analysis of peripheral blood mononuclear cells and adipose tissue cells from patients with CHIP and controls highlights differences at the cell type level. A. Peripheral blood mononuclear cells and adipose tissue cells from 6 patients with CHIP and 6 matched controls were analyzed using single-cell RNA sequencing and intercellular signaling prediction. Patients were matched on diabetic and HIV status. **B.** 73,790 cells represented in uniform manifold approximation and projection (UMAP) space. Cell type labels for PBMCs were assigned using scType, which relies on unsupervised clustering and known cell type marker genes. Cell types for adipose tissue cells were determined using unsupervised clustering and manual curation. Asterisk indicates cells are from blood. Otherwise, cells are from adipose tissue. **C.** Predicted differential signaling strength between cell types comparing CHIP to control. Line thickness is proportional to differential signaling strength. Largest differences in signaling strength seen in endothelial cells and macrophages.

Figure 2: Macrophages exhibit greater differences with CHIP than circulating CD14+ monocytes. A. Heatmap representing transcription factor enrichment for mutant and wildtype CD14+ monocytes (data originating from Heimlich et al 2023[8]). **B.** Volcano plots showing differential expression results comparing circulating CD14+ monocytes from patients with CHIP to circulating CD14+ monocytes from controls (left) and comparing macrophages from patients with CHIP to macrophages from controls (right). Differential expression was computed using a

metacells aggregation approach followed by a negative binomial Wald test with Benjamini Hochberg p-value adjustment. Genes highlighted in purple are involved in transendothelial migration. Genes highlighted in red are HLA types. **C.** Dotplot showing results of gene set enrichment analysis of differential expression for macrophages using all GO pathways.

Figure 3: Endothelial cells from patients with CHIP have altered gene expression and intercellular communication patterns. A. Volcano plot showing differential expression results comparing endothelial cells from patients with CHIP to endothelial cells from controls. Differential gene expression was computed using a metacells aggregation approach followed by a negative binomial Wald test with Benjamini Hochberg p-value adjustment. Genes highlighted in purple are involved in transendothelial migration. Genes highlighted in red are HLA types. **B.** Schematic showing key signaling molecules involved in transendothelial migration: chemokines/cytokines, selectins, integrins, and adhesion molecules. **C-F.** Predicted signaling strength for key pathways involved in transendothelial migration: CXCL, SELL, ITGB2, and PECAM1. Outgoing signaling from circulating CD14+ monocytes red, all other signaling in grey. Cell types with asterisks were captured in adipose tissue samples. Other cell types were captured in PBMCs. **G.** CellChat predicted signaling from circulating CD14+ monocytes to endothelial cells comparing CHIP to controls. Signaling for CXCL, SELL, ITGB2, and PECAM1 were all statistically significantly higher in CHIP than controls. Statistical significance was evaluated with a Wilcoxon test and the p-value significance threshold was adjusted using the Bonferroni correction (p-value < 0.0125, indicated by asterisk). **H.** CellChat predicted signaling from murine circulating monocytes from CHIP model mice and WT mice to healthy murine endothelial cells from the CZI CELLxGENE database. Statistical significance was evaluated with a Wilcoxon test and the p-value significance threshold was adjusted using the Bonferroni correction (p-value < 0.0125, indicated by asterisk). Not all signaling pathways were available for comparison between human and mouse data, so closely corresponding pathways were selected.

Figure 4: Macrophage-endothelial cell signaling has high heterogeneity depending on endothelial cell tissue of origin. A. Predictions were made based on interactions of macrophages from patients with CHIP and controls and endothelial cells from several tissues. Signaling predictions are based on expression of ligands, receptors, and cofactors. **B.** Within the adipose tissue dataset from this study, signaling between macrophages and endothelial cells differed for transendothelial migration pathways. Signaling was significantly higher for CXCL, ITGB2, and PECAM1 in CHIP compared to controls. Statistical significance was evaluated with a Wilcoxon test and the p-value significance threshold was adjusted using the Bonferroni correction (p-value < 0.017, indicated by asterisk). **C.** Predicted signaling strength from macrophages to endothelial cell from several tissues. Data originated from CZI CELLxGENE database. Line thickness is proportional to interaction strength. Asterisk indicates that data originated from this study. **D.** Ranked interaction strength between mutant CD14+ monocytes and endothelial cells from several tissues. Asterisk indicates that data originated from this study. **E.** Heatmap for transcription factor enrichment of high and low interacting endothelial cells from CHIP adipose tissue samples. **F.** Predicted signaling from CHIP and control macrophages to high and low interacting endothelial cells from CHIP adipose tissue samples for CXCL signaling. **G.** Boxplot showing high interactor proportions for subtypes of endothelial cells. Venous endothelial cell status is a positive predictor of high interactor status (generalized linear model coefficient = 0.461, standard error = 0.138, p-value = 0.004). Dots of the same color are from the same patient.

Supplementary Figure 1: CD14+ monocyte and macrophage UMAP. UMAP demonstrating separation of circulating CD14+ monocytes, adipose tissue CD14+ monocytes, and macrophages.

Supplementary Figure 2: CD14+ monocytes gene set enrichment. Dotplot showing results of gene set enrichment analysis of differential expression for CD14+ monocytes using all GO pathways.

Supplementary Figure 3: Endothelial cell marker expression for data from CZI CELLxGENE. Dotplot showing average expression and percent expression for known endothelial cell markers in CZI data.

Table 1: Demographic characteristics for patients with matched PBMC and adipose tissue samples. Table displaying sex, age, study group, and BMI for cases and controls.

Supplementary Table 1: Differential expression results comparing macrophages from patients with CHIP and from controls.

Supplementary Table 2: Differential expression results comparing adipose tissue circulating CD14+ monocytes from patients with CHIP and from controls.

Supplementary Table 3: Differential expression results comparing endothelial cells from patients with CHIP and from controls.

Supplementary Table 4: Marker genes defining high interactor and low interactor endothelial cells.

Code availability: All code used in this analysis has been deposited on GitHub at https://github.com/bicklab/SC_CHIP_HIV_Diabetes and will be made public at the time of publication.

Data availability: Data generated in this analysis will be made available on the Chan Zuckerberg Initiative's CELLxGENE database upon publication.

Graphical abstract

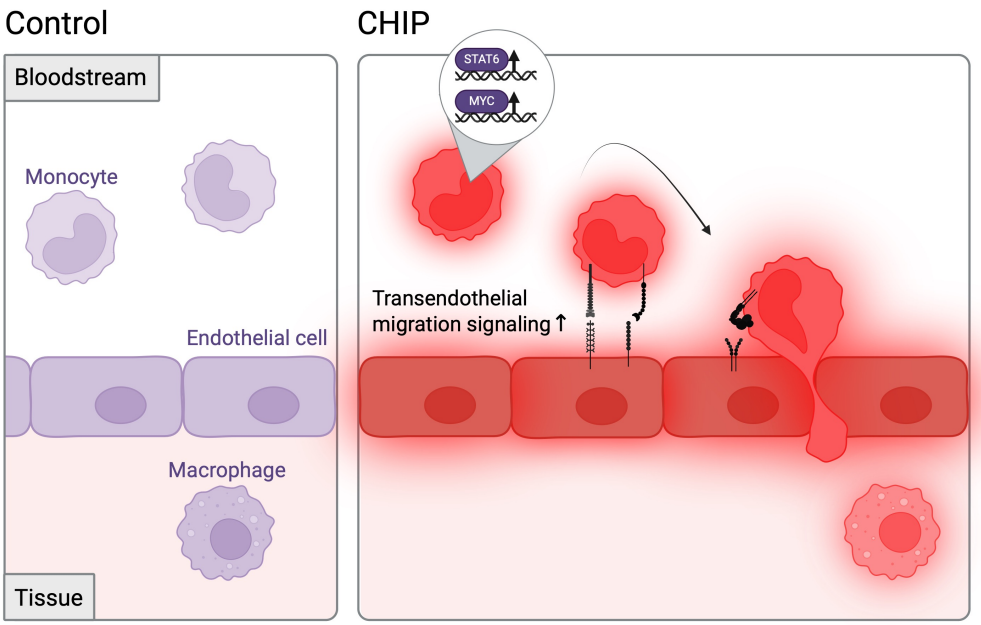

Figure 1

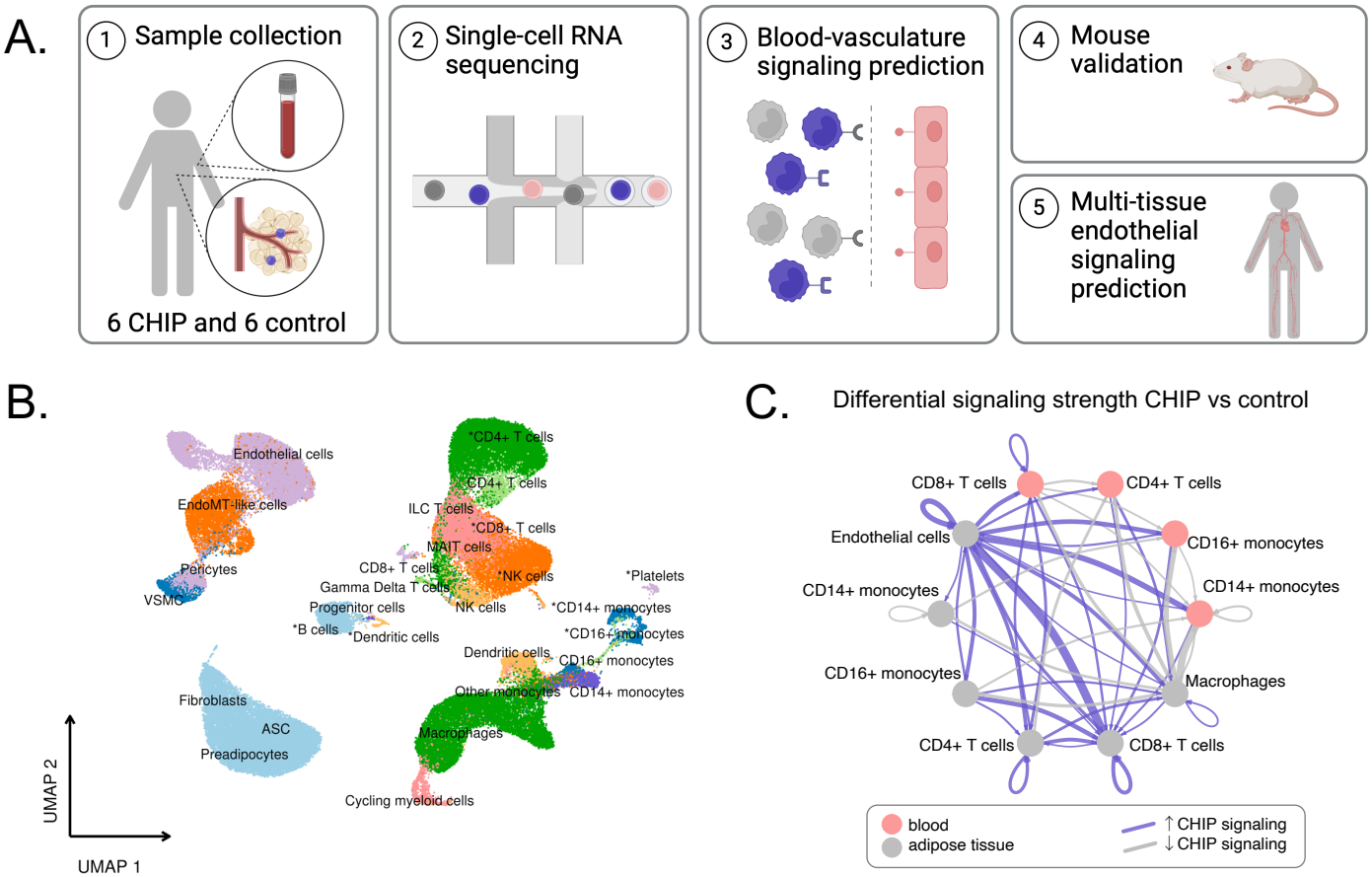

Figure 1: Single-cell analysis of peripheral blood mononuclear cells and adipose tissue cells from patients with CHIP and controls highlights differences at the cell type level. A. Peripheral blood mononuclear cells and adipose tissue cells from 6 patients with CHIP and 6 matched controls were analyzed using single-cell RNA sequencing and intercellular signaling prediction. Patients were matched on diabetic and HIV status. **B.** 73,790 cells represented in uniform manifold approximation and projection (UMAP) space. Cell type labels for PBMCs were assigned using scType, which relies on unsupervised clustering and known cell type marker genes. Cell types for adipose tissue cells were determined using unsupervised clustering and manual curation. Asterisk indicates cells are from blood. Otherwise, cells are from adipose tissue. **C.** Predicted differential signaling strength between cell types comparing CHIP to control. Line thickness is proportional to differential signaling strength. Largest differences in signaling strength seen in endothelial cells and macrophages.

Figure 2

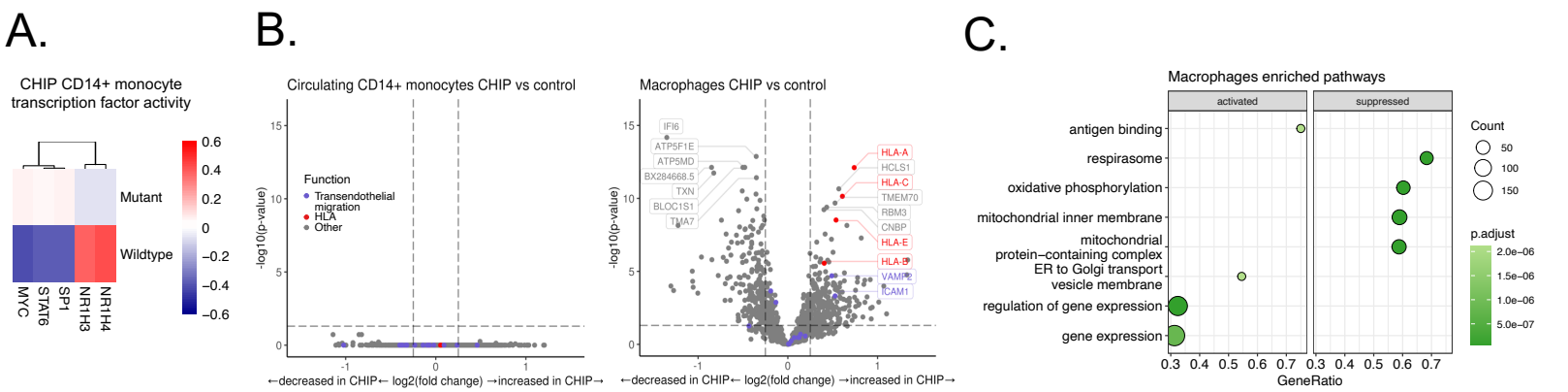

Figure 2: Macrophages exhibit greater differences with CHIP than circulating CD14+ monocytes. A. Heatmap representing transcription factor enrichment for mutant and wildtype CD14+ monocytes (data originating from Heimlich et al 2023[8]). **B.** Volcano plots showing differential expression results comparing circulating CD14+ monocytes from patients with CHIP to circulating CD14+ monocytes from controls (left) and comparing macrophages from patients with CHIP to macrophages from controls (right). Differential expression was computed using a metacells aggregation approach followed by a negative binomial Wald test with Benjamini Hochberg p-value adjustment. Genes highlighted in purple are involved in transendothelial migration. Genes highlighted in red are HLA types. **C.** Dotplot showing results of gene set enrichment analysis of differential expression for macrophages using all GO pathways.

Figure 3

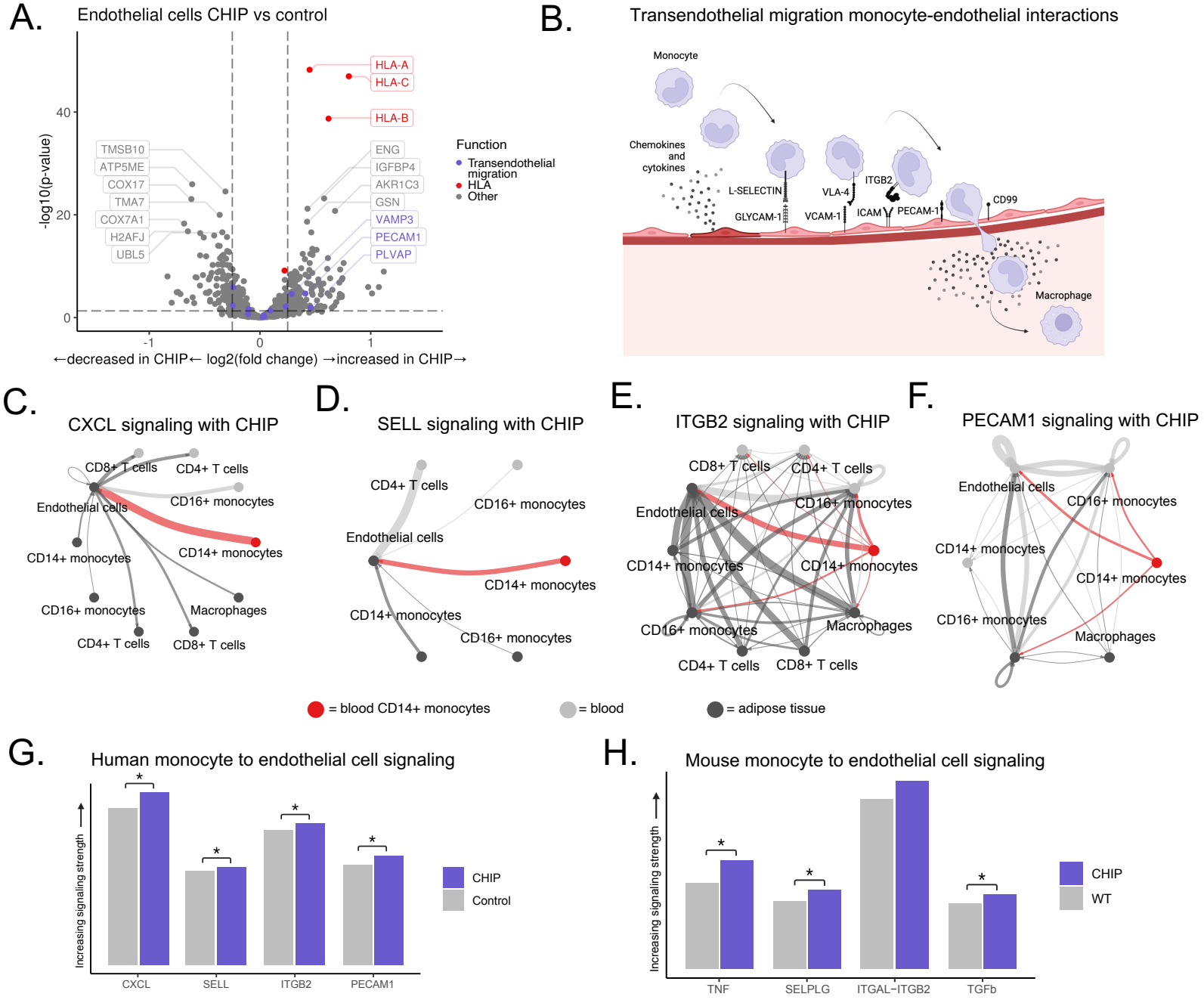

Figure 3: Endothelial cells from patients with CHIP have altered gene expression and intercellular communication patterns. A. Volcano plot showing differential expression results comparing endothelial cells from patients with CHIP to endothelial cells from controls. Differential gene expression was computed using a metacells aggregation approach followed by a negative binomial Wald test with Benjamini Hochberg p-value adjustment. Genes highlighted in purple are involved in transendothelial migration. Genes highlighted in red are HLA types. **B.** Schematic showing key signaling molecules involved in transendothelial migration: chemokines/cytokines, selectins, integrins, and adhesion molecules. **C-F.** Predicted signaling strength for key pathways involved in transendothelial migration: CXCL, SELL, ITGB2, and PECAM1. Outgoing signaling from circulating CD14+ monocytes red, all other signaling in grey. Cell types with asterisks were captured in adipose tissue samples. Other cell types were captured in PBMCs. **G.** CellChat predicted signaling from circulating CD14+ monocytes to endothelial cells comparing CHIP to controls. Signaling for CXCL, SELL, ITGB2, and PECAM1 were all statistically significantly higher in CHIP than controls. Statistical significance was evaluated with a Wilcoxon test and the p-value significance threshold was adjusted using the Bonferroni correction (p-value < 0.0125, indicated by asterisk). **H.** CellChat predicted signaling from murine circulating monocytes from CHIP model mice and WT mice to healthy murine endothelial cells from the CZI CELLxGENE database. Statistical significance was evaluated with a Wilcoxon test and the p-value significance threshold was adjusted using the Bonferroni correction (p-value < 0.0125, indicated by asterisk). Not all signaling pathways were available for comparison between human and mouse data, so closely corresponding pathways were selected.

Figure 4

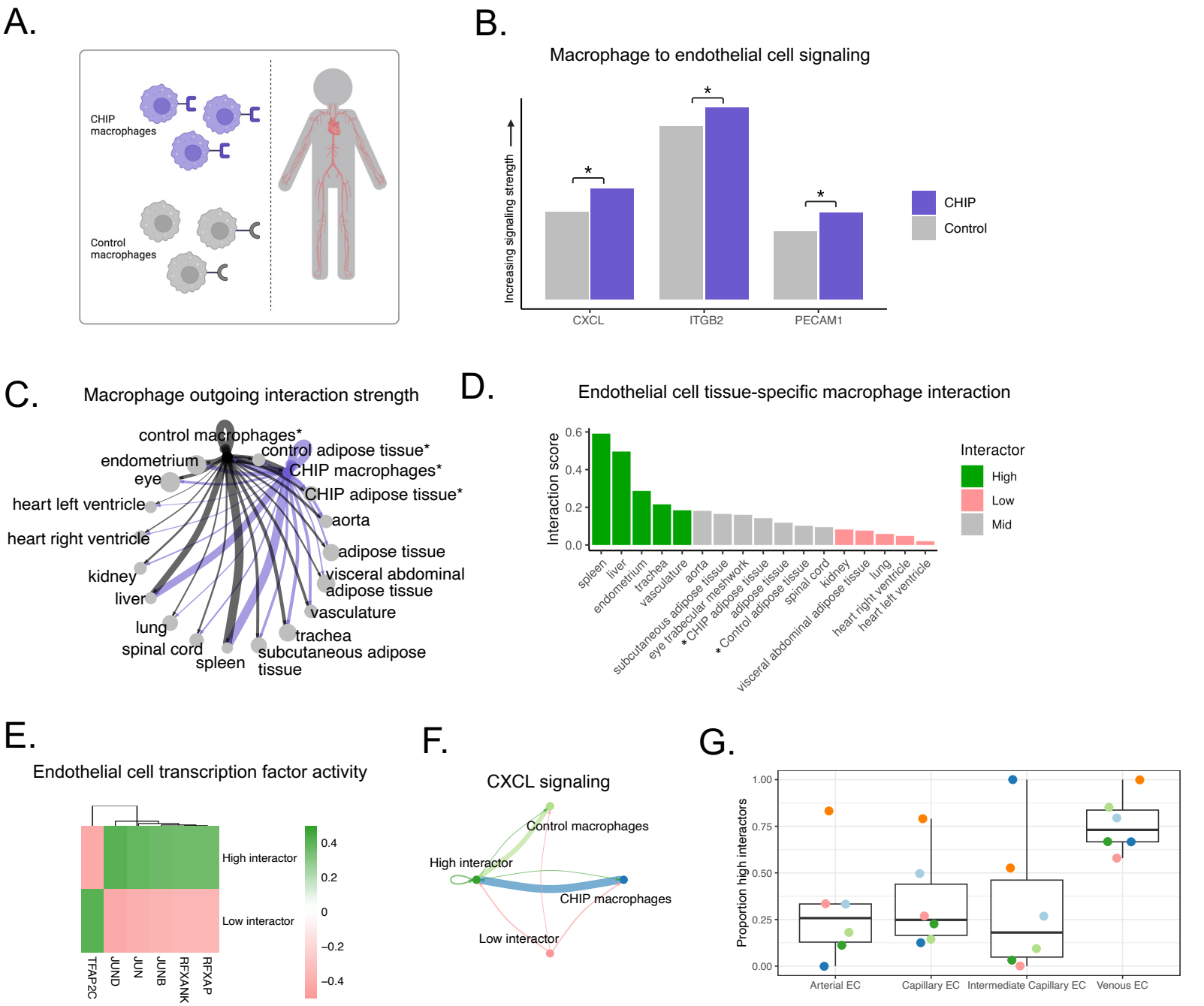

Figure 4: Macrophage-endothelial cell signaling has high heterogeneity depending on endothelial cell tissue of origin. A. Predictions were made based on interactions of macrophages from patients with CHIP and controls and endothelial cells from several tissues. Signaling predictions are based on expression of ligands, receptors, and cofactors. **B.** Within the adipose tissue dataset from this study, signaling between macrophages and endothelial cells differed for transendothelial migration pathways. Signaling was significantly higher for CXCL, ITGB2, and PECAM1 in CHIP compared to controls. Statistical significance was evaluated with a Wilcoxon test and the p-value significance threshold was adjusted using the Bonferroni correction (p-value < 0.017, indicated by asterisk). **C.** Predicted signaling strength from macrophages to endothelial cell from several tissues. Data originated from CZI CELLxGENE database. Line thickness is proportional to interaction strength. Asterisk indicates that data originated from this study. **D.** Ranked interaction strength between mutant CD14+ monocytes and endothelial cells from several tissues. Asterisk indicates that data originated from this study. **E.** Heatmap for transcription factor enrichment of high and low interacting endothelial cells from CHIP adipose tissue samples. **F.** Predicted signaling from CHIP and control macrophages to high and low interacting endothelial cells from CHIP adipose tissue samples for CXCL signaling. **G.** Boxplot showing high interactor proportions for subtypes of endothelial cells. Venous endothelial cell status is a positive predictor of high interactor status (generalized linear model coefficient = 0.461, standard error = 0.138, p-value = 0.004). Dots of the same color are from the same patient.

Supplemental Figure 1

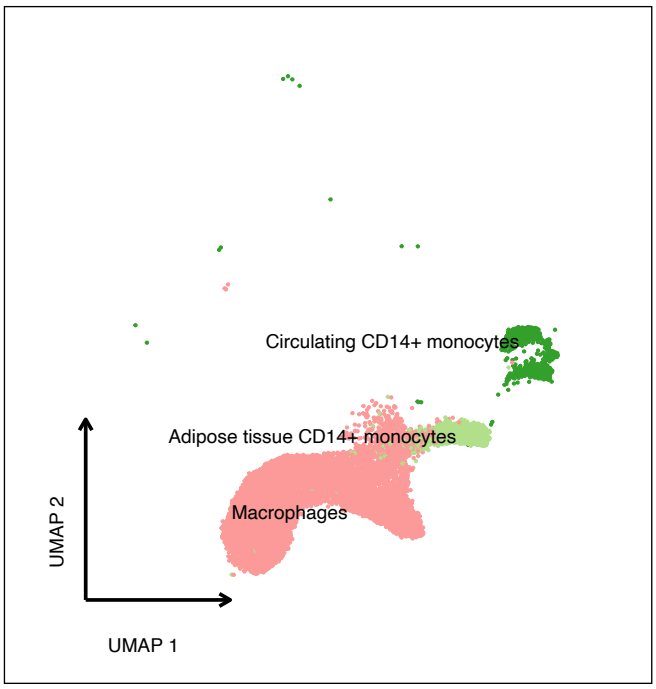

Supplementary Figure 1: CD14+ monocyte and macrophage UMAP. UMAP demonstrating separation of circulating CD14+ monocytes, adipose tissue CD14+ monocytes, and macrophages.

Supplemental Figure 2

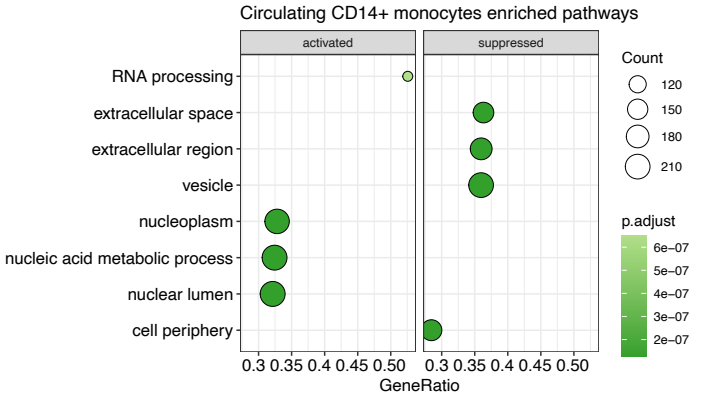

Supplementary Figure 2: CD14+ monocytes gene set enrichment. Dotplot showing results of gene set enrichment analysis of differential expression for CD14+ monocytes using all GO pathways.

Supplemental Figure 3

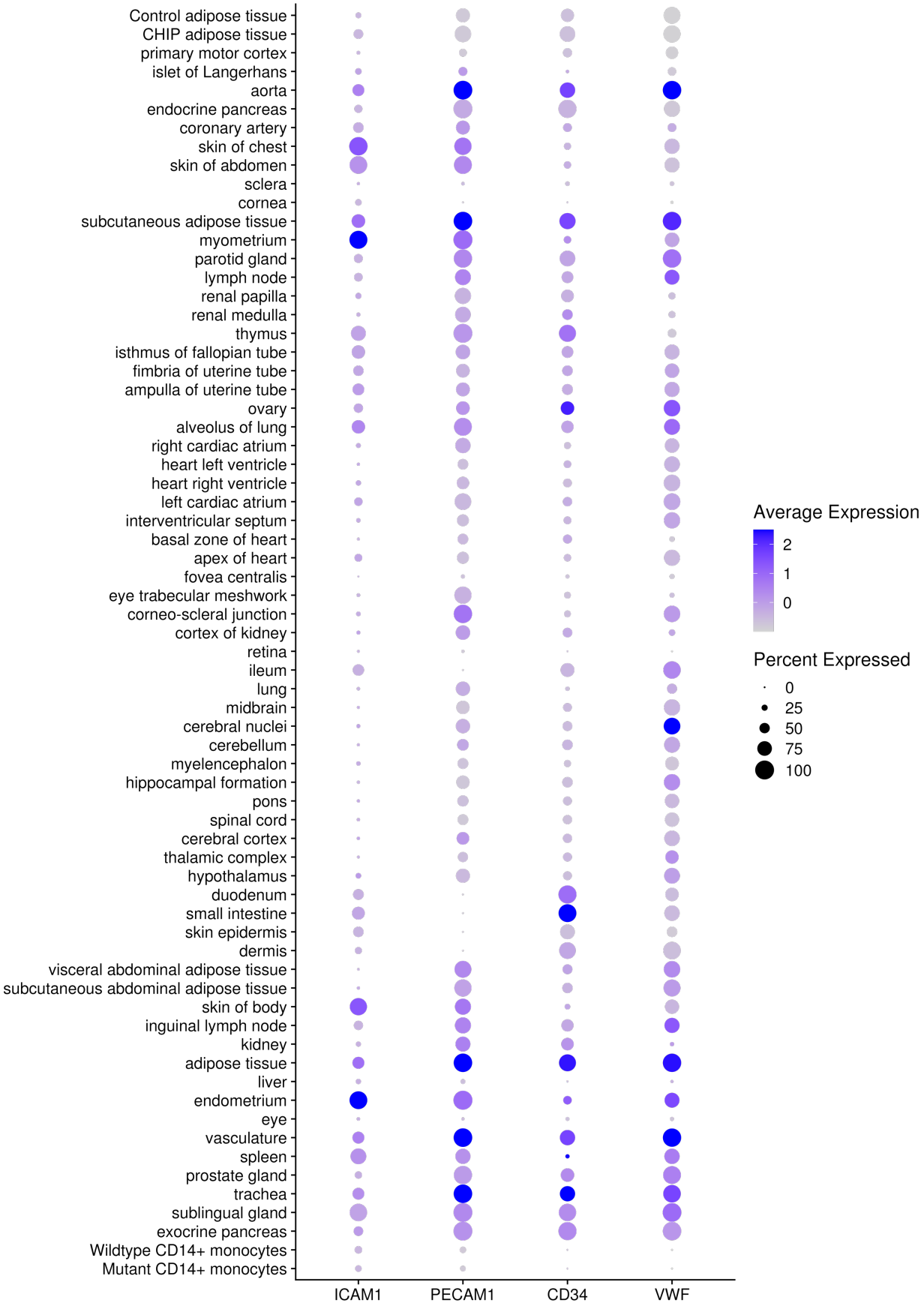

Supplementary Figure 3: Endothelial cell marker expression for data from CZI CELLxGENE. Dotplot showing average expression and percent expression for known endothelial cell markers in CZI data.

Table 1

		CHIP (n = 6)	Control (n = 6)
Sex	Female	3 (50%)	3 (50%)
	Male	3 (50%)	3 (50%)
Age	Mean (SD)	55 (9.8)	56 (8.8)
Study Group	HIV- diabetic	5 (83.3%)	5 (83.3%)
	HIV+ prediabetic	1 (16.7%)	1 (16.7%)
BMI	Mean (SD)	39 (7.2)	40 (9.0)

Table 1: Demographic characteristics for patients with matched PBMC and adipose tissue samples. Table displaying sex, age, study group, and BMI for cases and controls.